2024 IEEE/RSJ International Conference on Intelligent Robots and Systems (IROS)
October 14-18, 2024. Abu Dhabi, UAE

Millipede-Inspired Multi-legged Magnetic Soft Robots for Targeted Locomotion in Tortuous Environments

Yibin Wang, *Student Member, IEEE*, Yiting Xiong, Kaiwen Fang, *Student Member, IEEE*, and Jiangfan Yu, *Member, IEEE*

Abstract— **Miniature robots capable of untethered operation hold great promise for performing diagnostic and therapeutic procedures in hard-to-reach regions within the human body. Nonetheless, navigating these complex and diverse physiological environments remains a significant challenge. To effectively navigate the tortuous pathways inside the human body, it is essential to equip miniature robots with flexible body structures that can adapt to complex geometries and develop efficient actuation strategies for deformed robots. In this study, we present a miniature soft robot featuring a zigzag body structure, imparting the robot with remarkable deformation capabilities that enable it to adapt to confined and tortuous spaces. This robot is equipped with arrays of magnetic legs, enabling robust locomotion propelled by traveling metachronal waves. We demonstrate that the robot can crawl on both flat surfaces and slopes. Leveraging its in-plane flexibility and discrete actuation system, this robot can navigate through intricate environments with precise control using magnetic fields. Our work provides valuable insights into the development of crawling robots with enhanced agility and adaptability, creating opportunities for their future use in a wide range of biomedical applications.**

I. Introduction

The remarkable attributes of soft robots, such as enhanced flexibility, adaptability, and biocompatibility compared to their rigid counterparts, have elicited significant interest for potential biomedical applications [1]. Specifically, when miniaturized to the millimeter scale and operated wirelessly, these soft robots offer noninvasive access to inaccessible regions within the human body, facilitating therapeutic interventions and diagnostic procedures [2-6]. Several actuation techniques have been developed for controlling untethered miniature soft robots [7-10]. Among these methods, magnetic manipulation shows immense promise due to its ability to safely penetrate the human body and enable precise manipulation of magnetic objects [11-13].

Drawing inspiration from living organisms, enormous advancements have been made in recent years on magnetic soft miniature robots [14-20]. For example, inspired by the movement of jellyfish, Ren et al. [21] developed a soft millirobot that performs a swimming gait resembling the ephyra jellyfish. Dong et al. [22] investigated the non-reciprocal motion of bioinspired cilia arrays. Gu et al. [23] developed cilia carpets with programmed metachronal waves, which demonstrate applications in fluidic manipulation. Inspired by fish, undulatory miniature swimmers are also developed [24-26]. The potential implementation of magnetic miniature robots in physiological environments is also investigated. For example, Ren et al. [27] investigated the adaptive locomotion of magnetic soft robots in fluid-filled confined spaces. Wu et al. [28] developed a millirobot capable of climbing on mucus-covered tissue surfaces. These magnetic soft robots have great potential in biomedical applications, such as in-situ sensing [29], drug delivery [30], and embolization [31]. However, terrestrial miniature robots that can navigate inside tortuous and confined cavities have not been demonstrated. Such robots may play important roles in biomedical-related tasks implemented in empty orifices inside the human body.

In this work, a millipede-inspired magnetic soft robot capable of navigating tortuous and confined environments is developed. The robot design is inspired by the propulsion mechanism and body configuration of the millipede. Millipedes adopt unique metachronal waves for propulsion. The metachronal wave generation is replicated by the robot with arrays of magnetic legs magnetized with sequential phase differences. Furthermore, as a kind of annelid, the body of millipedes is divided into segments by flexible transverse rings. Such a unique structure ensures the flexibility of millipedes despite their hard exoskeleton. Mimicking such body structure, the robot body is designed with a zigzag shape, with repeated leg-bearing segments and linkers, which endows the robot with in-plane flexibility. The metachronal wave propulsion strategy and flexibility allow it to adapt to tortuous and confined cavities under magnetic actuation.

II. Design and Fabrication

A. Design of the Robot

Inspired by the millipede in nature, the robot is designed with a non-magnetic body and two arrays of magnetic legs on two sides of its body. To increase the flexibility of the robot in its body plane, we design a body with a zigzag pattern. The bending stiffness K of the body can be described as: $K = EI$, where E is the Young's modulus, I is the second moment of inertia of the cross-sectional area. With the zigzag pattern, the cross-sectional area of the body part is significantly decreased, which reduces the bending stiffness of the robot body.

* This work was supported in part by the National Natural Science Foundation of China under Grant 62103347, in part by the Shenzhen Science and Technology Innovation Program under Grant RCBS20210609103155061, Guangdong Basic and Applied Basic Research Foundation under Grant 2023A1515012973 and Grant 2022A1515110499, and in part by the Shenzhen Institute of Artificial Intelligence and Robotics for Society.

The authors are with the School of Science and Engineering, The Chinese University of Hong Kong, Shenzhen 518172, China.

Yibin Wang, Kaiwen Fang, and Jiangfan Yu are also with the Shenzhen Institute of Artificial Intelligence and Robotics for Society (AIRS), Shenzhen 518129, China.

(Yibin Wang and Yiting Xiong contributed equally to this work.) (Corresponding author: Jiangfan Yu, email: yujiangfan@cuhk.edu.cn).

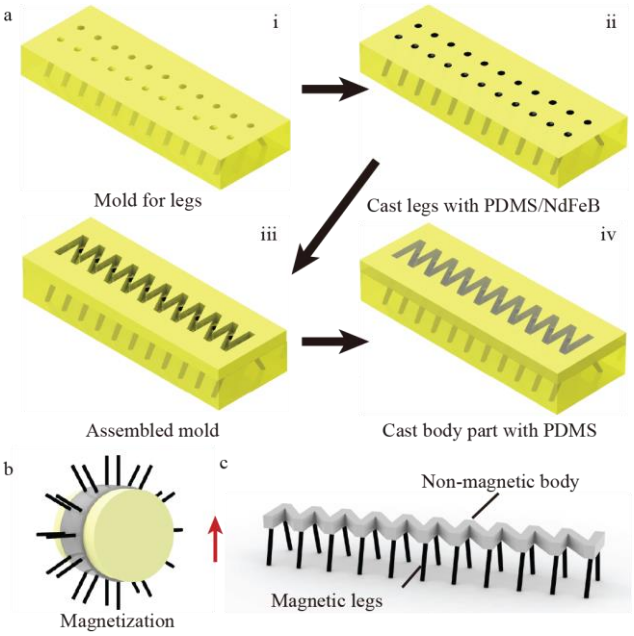

Figure 1. Fabrication and magnetization of the robot. (a) The two-step mold casting method. (b) The magnetization configuration of the robot. (c) The model of the robot after being released from the mold.

For generating metachronal waves mimicking millipede, we configure 11 legs on each side of the robot, with each leg designed to have a length of 3 mm and a diameter of 0.55 mm. The spacing between the legs is set at 1.7 mm, and there is a 3 mm separation between the two arrays. The body length of the robot is 20 mm. Based on these parameters, three types of robots with different leg angles (β), i.e., 0°, 15°, and 30°, are designed and fabricated. Here, the leg angle β is defined as the angle between the legs and the vertical direction. To investigate the influence of leg stiffness on crawling motion, robots with legs of different stiffness are fabricated. The robots with stiffer legs are designated as type A robots, while the robots with softer legs are designated as type B robots. To simplify identification, we adopt a naming convention that combines the leg angle and stiffness. For example, Robot-15-A represents the robot with a leg angle of 15° and a higher Young's modulus. In subsequent sections, we will delve into the relationship between leg angle, leg stiffness, and their influence on crawling performance.

B. Materials

The robots are constructed with two components, i.e., non-magnetic bodies and magnetic legs. The material used for the non-magnetic body is PDMS (SYLGARD 184 silicone elastomer kit, Dow Corning) prepared by mixing base and curing agent of Sylgard 184 in a 10:1 weight ratio. The material used for the magnetic legs is PDMS embedded with neodymium-iron-boron (NdFeB) magnetic particles (MQFP-15-7, Magnequench). To vary the stiffness of the magnetic legs, we adjust the ratio between the base and curing agents. Type A robots, characterized by stiffer legs, maintain a base-to-curing agent ratio of 10:1, while Type B robots, featuring softer legs, utilize a ratio of 15:1. In both robot types, the NdFeB weight fraction remains consistent at 50%.

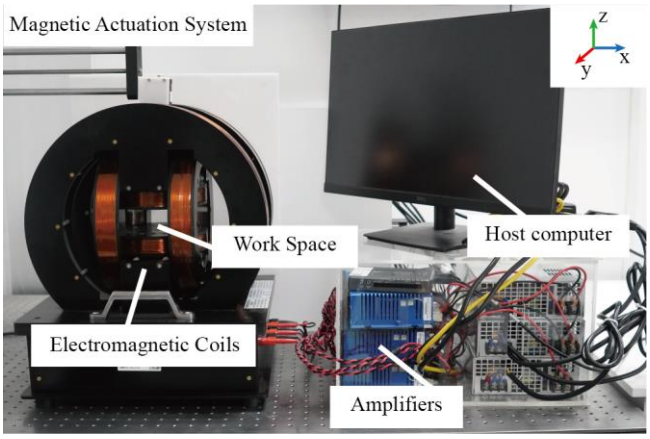

Figure 2. Magnetic actuation system. Image of the three-axis Helmholtz coil, control box and host computer.

The mechanical strength of the magnetic legs is characterized by the tensile test. The resulting Young's modulus of the Type A robot and Type B robot are 224 ± 10 KPa and 186 ± 13 KPa, respectively.

C. Fabrication of the Robot

The robot is fabricated with a two-step mold casting method (Fig. 1(a)). The molds are 3D-printed with a projection-micro-stereolithography printer (BMF P150). To prepare the resin mold for use, it undergoes a thorough cleaning step involving a 30-minute immersion in IPA to eliminate any remaining uncured resin, followed by a 2-hour post-curing step at 100°C. Before introducing the PDMS prepolymer, a release agent is applied to the surface of the mold to facilitate smooth demolding.

In the first step, the mixture of PDMS prepolymer and NdFeB is first filled in the mold under vacuum for 15 minutes. Subsequently, the leg part is allowed to cure in an oven at 80 C° for 30 minutes. Then the excess composite is removed, and the mold for the robot body is assembled on top of the initial mold. The PDMS prepolymer is then filled into the second mold. The whole setup is again cured in an oven at 80 C° for 30 minutes. After fully curing, the robot is released from the mold and magnetized with a magnetizer (Fig. 1(b,c)).

III. Modeling

A. Magnetic Actuation

A three-axis Helmholtz coil is used for magnetic actuation (Fig. 2). The setup can generate a uniform magnetic field up to 20 mT in a workspace with dimensions of 8 cm × 8 cm ×4 cm.

The robot is actuated by a rotating magnetic field. The plane of the rotating magnetic field is perpendicular to the x-y plane. The direction angle α determines the angle between the rotating plane and the x-axis. The clockwise rotating magnetic field with strength $\boldsymbol{A}$, frequency f, and direction angle α can be expressed as:

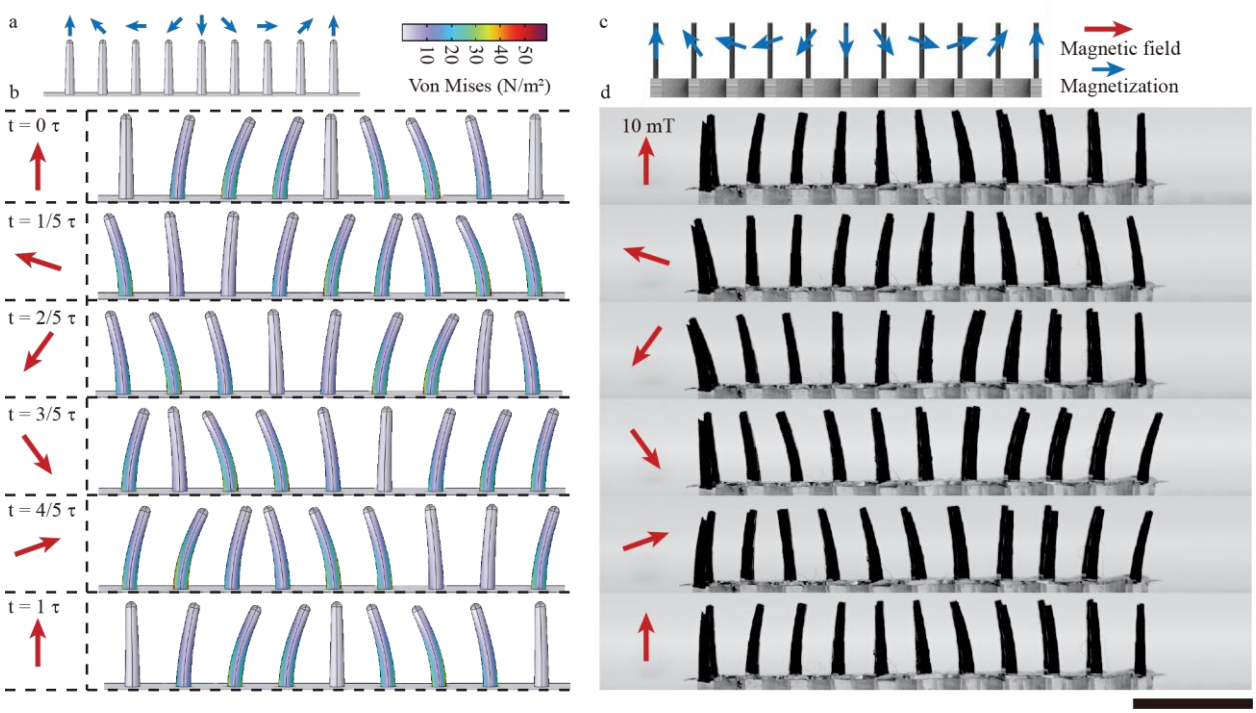

Figure 3. Metachronal wave generation. (a) The magnetization profile of the simulated array of magnetic legs. The blue arrows indicate the magnetization direction. (b) The simulated deformation of the array of magnetic legs at different times in one actuation cycle. The red arrows indicate the direction of the applied magnetic field. The color bar shows the stress on the deformed magnetic legs. (c) The magnetization profile of the robot legs. (d) The deformation of the robot legs under a magnetic field with varying directions.Scale bar: 5 mm

$$\boldsymbol{B}(t)=\begin{pmatrix} A\cos\alpha\sin(2\pi ft)\hat{\boldsymbol{e}}_x \\ -A\sin\alpha\sin(2\pi ft)\hat{\boldsymbol{e}}_y \\ A\cos(2\pi ft)\hat{\boldsymbol{e}}_z \end{pmatrix} \tag{1}$$

where $\hat{\mathbf{e}}_x$, $\hat{\mathbf{e}}_y$, $\hat{\mathbf{e}}_z$ represents the unit vector in the x-axis, y-aixs, z-aixs respectively.

B. *Quasi-static Analysis*

As mentioned above, the robot is magnetized being fixed on a curved template (Fig. 1(b)), which results in a single wavelength harmonic magnetization profile in the magnetic legs along its body. The magnetization $\boldsymbol{m}$ of each leg can be described as:

$$\boldsymbol{m}=\begin{pmatrix} m_x \\ m_y \\ 0 \end{pmatrix}=m\begin{pmatrix} \cos\theta_m \\ \sin\theta_m \\ 0 \end{pmatrix} \tag{2}$$

where θ_m is defined as the magnetization direction of induvidual legs. Under the external magnetic field, $\boldsymbol{B}=\begin{bmatrix} B_x B_y B_z \end{bmatrix}^{\mathrm{T}}$, magnetic torque τ_m can be generated. The magnetic torque τ_m can thus be expressed as:

$$\tau_m=\boldsymbol{m}\times\boldsymbol{B} \tag{3}$$

The resulting deformation of the individual legs with deflection Δ and length s can be modeled by Euler-Bernoulli equation as:

$$M=EI\frac{\partial^2\Delta}{\partial s^2} \tag{4}$$

where M represents the bending moment, E represents the Young's modulus, and I represents the second moment of area. Based on the above theory, the deformation of individual legs induced by magnetic torque can be simulated with finite element analysis.

Based on the simulated deformation of individual legs, we further simulated the deformation of an array of magnetic legs with single-wavelength harmonic magnetization profiles in the rotating magnetic field. In the simplified model, we designed an array of magnetic legs with 9 legs, each leg has a length of 3 mm and a diameter of 0.55 mm. The magnetization directions of the legs are set from 0° to 360° with increments of 45° (Fig. 3(a)). As the magnetic field direction rotates counterclockwise, the metachronal wave generates and propagates from left to right (Fig. 3(b), Supplementary Video 1).

IV. Experiment Results

A. *Metachronal Wave Generation*

The metachronal wave is generated by actuating the magnetic robot with a rotating magnetic field. Since the legs of the robot possess a single-wavelength harmonic magnetization

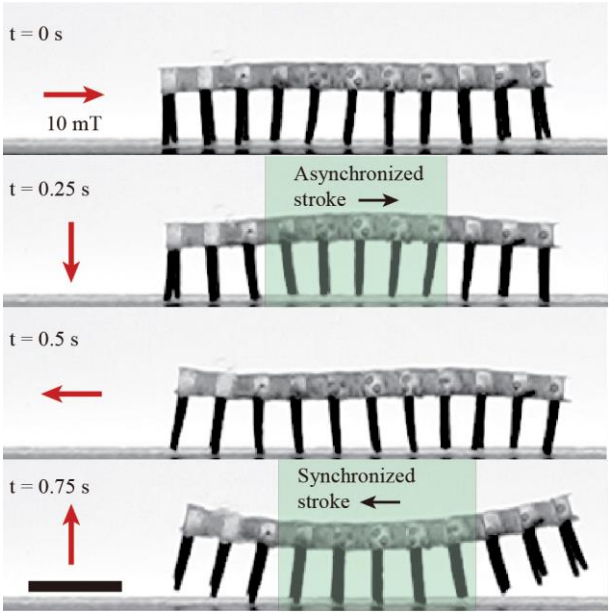

Figure 4. Gait analysis. The snapshots of the robot in one crawling cycle. The red arrows indicate the direction of the magnetic field, The black arrows indicate the stroke direction of the robot legs. Scale bar: 5 mm.

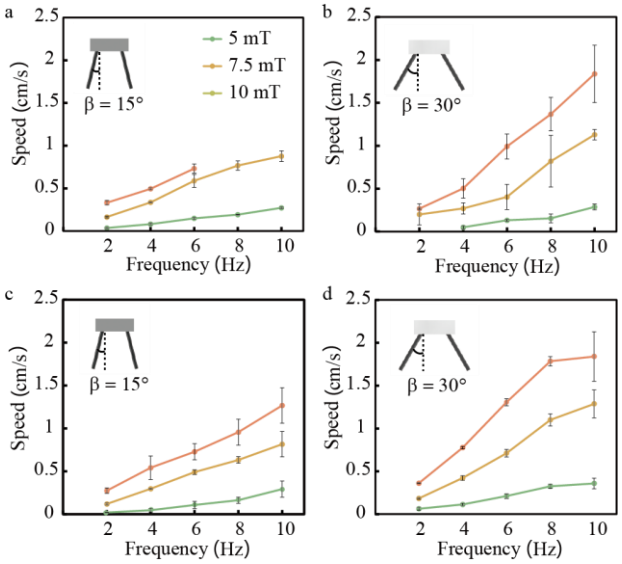

Figure 5. Characterization of the robot locomotion. The Crawling speed of Robot-15-A (a), Robot-30-A (b), Robot-15-B (c), and Robot-30-B (d).

profile, they are actuated in phase under a rotating magnetic field, thereby generating the metachronal wave. The motion of legs during one complete rotation cycle can be divided into two phases: the synchronized phase, during which magnetic torque prevails, the robot legs deform following the magnetic field; and the asynchronized phase, where elasticity dominates, causing the robot legs to rebound due to elastic recovery.

To validate the generation of the metachronal wave, we actuated the robot with a leg angle of 0° in a rotating magnetic field. Upon applying a counterclockwise rotating magnetic field, the metachronal wave is generated and propagates from left to right (Fig. 3(d)). The experimental results align closely with the simulation results. Here, we define the synchronized phase as the power stroke and the asynchronized phase as the recovery stroke. Depending on the direction of wave propagation and the power stroke, the metachronal wave can be categorized into two types: the symplectic metachronal wave, where wave propagation and the power stroke share the same direction; and the antiplectic metachronal wave, where they have opposite directions. Utilizing the magnetization method illustrated in Fig. 2(b), we encode the magnetization profile that generates the antiplectic wave in the robot.

B. Locomotion with Metachronal Waves

In nature, millipedes adopt a metachronal gait through the coordinated movement of their legs, generating a traveling wave from their tail to their head. During the metachronal gait, the legs make contact with the ground in the power stroke and then break contact with the ground by lifting its legs in the recovery stroke. In such a way, the discrete motions of individual legs collectively contribute to the overall thrust. In millipede locomotion, the metachronal propagation direction is opposite to the power stroke direction. To mimic the metachronal gait of millipedes, we adopt the antiplectic metachronal wave to generate thrust.

The locomotion mechanism is first investigated using the robot with a leg angle of 30°. The robot is actuated by a clockwise rotating magnetic field with a strength of 10 mT and a frequency of 1 Hz. We observe that the robot locomotion is achieved through the coupling effects between the metachronal wave and its body deformation.

Since the body of the robot is flexible, the torque exerted on the robot legs also deforms the body. In the rotating magnetic field, the body of the robot changes its curvature along with the traveling wave, which is key to achieve net displacement. In one actuation cycle, i.e., the magnetic field rotates 360°, the body of the robot first changes from a flat configuration (Fig. 4, 0 s) to a concave configuration (Fig. 4, 0.25 s), during which the middle legs of the robot are elevated and perform an asynchronized stroke forward. Since the legs do not contact the ground, there is no backward thrust caused by the asynchronized stroke. Subsequently, the body of the robot changes back to a flat configuration (Fig. 4, 0.5 s), and the middle legs contact the ground. During the further transformation from a flat configuration to a convex configuration (Fig. 4, 0.75 s), these middle legs perform a synchronized stroke, providing forward thrust for the robot. The net displacement resulting from the collective contributions of these discrete motions is thus generated.

To further investigate the influence of structure and actuation strategy on locomotion efficiency, robots with varying leg angles and stiffness are fabricated. The moving speed of these robots under a rotating magnetic field with varying strength and frequency is characterized (Fig. 5). The experiment results indicate that robots with softer legs have better performance than robots with stiffer legs. As the robot legs become softer, both the maximum speed and stability increase, which we attribute to their larger stroke range.

We also observe that robots with a larger leg angle (30°) exhibit higher speed compared to those with a smaller leg

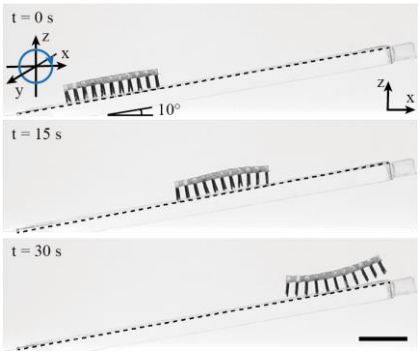

Figure 6. Locomotion of the robot on a slope. Snapshot of the robot climbing a slope with a 10° incline. Scale bar: 10 mm.

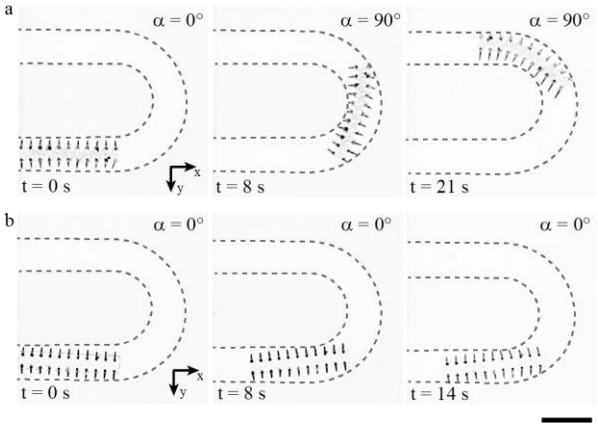

Figure 7. Locomotion of the robots in a U-shaped channel. (a) The robot with a zigzag body configuration crawls through the U-shaped channel. (b) The robot with a straight body gets stuck in the U-shaped channel. Scale bar: 10 mm.

angle (15°). Robot-30-B achieves a maximum speed of 1.8 cm/s, approximately 1 body length per second. Regarding magnetic actuation, the results suggest that as the magnetic field strength and frequency of the rotating magnetic field increase, the crawling speed of the robot also increases.

To further verify the propulsion efficiency of the robot, we demonstrate its ability to climb a slope with a 10° incline actuated by a rotating magnetic field with a strength of 10 mT and a frequency of 2 Hz (Fig. 6, Supplementary Video 2). The robot continued to utilize the traveling metachronal wave for locomotion. However, due to the gravitational force, the locomotion efficiency is compromised, resulting in reduced speed.

C. Locomotion in Tortuous Environment

Since the robot can be controlled wirelessly by external magnetic fields and perform robust and efficient locomotion, it shows great potential in biomedical applications. When navigating inside the human body, the surrounding environment is usually narrow and tortuous, demanding improved adaptability of the robot. Currently, most existing soft robots only show the degree of freedom perpendicular to their body plane, allowing them to traverse confined spaces with height limitations. However, when faced with narrow spaces with sharp turns within their body plane, flexibility in that plane is essential for the robot to adapt and maneuver effectively. Furthermore, efficient propulsion becomes challenging for magnetic soft robots when they deform, as magnetic fields typically provide directional propulsion that may not be suitable for actuating robots in curved configurations. These two challenges can be effectively addressed by the proposed robot. First of all, the body of the robot is designed with a zigzag pattern that greatly reduces its cross-sectional area, thereby decreasing its bending stiffness within its body plane. Consequently, the robot can easily deform to adapt to a tortuous environment. Moreover, the thrust for propelling the robot is generated through the discrete motion of its legs. This discrete system offers a more robust actuation strategy compared to robots with continuous actuators. Even if external magnetic actuation may not be optimal for all the legs, they can still achieve the desired locomotion.

To verify the capability of the robot in navigating tortuous landscapes, we prepared a channel with a U-shaped turn (Fig. 7). The width of the channel is 6 mm, slightly larger than the width of the robot, i.e., 4.8 mm. The robot is first actuated with a rotating magnetic field in the x-z plane with a direction angle of 0°. Under the clockwise rotating magnetic field, the robot moves in the x direction and enters the U-shaped turn. Leveraging its flexible body, the robot can passively deform to fit the curved channel. As the robot enters the U-shaped turn, even though the stroke direction of the robot legs is no longer aligned with the forward direction, they still provide thrust that pushes the robot through the channel. The rotating magnetic field with a direction angle of 0° can guide the robot to take a maximum 90° turn based on the geometry of the channel. When the robot body becomes perpendicular to the rotating magnetic field, no net displacement can be generated because the stroke direction of all the legs is perpendicular to the desired forward direction, resulting in no thrust force for the robot locomotion. To proceed, the rotating magnetic field is adjusted to the y-z plane, where the robot body is aligned. This allowed the robot to begin moving again until its body completed the U-shaped turn. Subsequently, a rotating magnetic field in the x-z plane with a direction angle of 180° can be used to actuate the robot out of the channel (Supplementary Video 3).

To investigate the influence of the bending stiffness on the adaptability of the robot to a tortuous landscape. A robot with a straight body is prepared. The same magnetic actuation is applied to propel the robot in the U-shaped channel. However, due to its limited flexibility in its body plane, the robot can not deform to fit into the channel, and thus cannot complete the U-turn under the same magnetic field.

Then we demonstrate that the robot can be navigated to walk through a more complex channel with sharp turns, achieved by adjusting the direction angle of the rotating magnetic field to align with the body of the robot (Fig. 8, Supplementary Video 4).

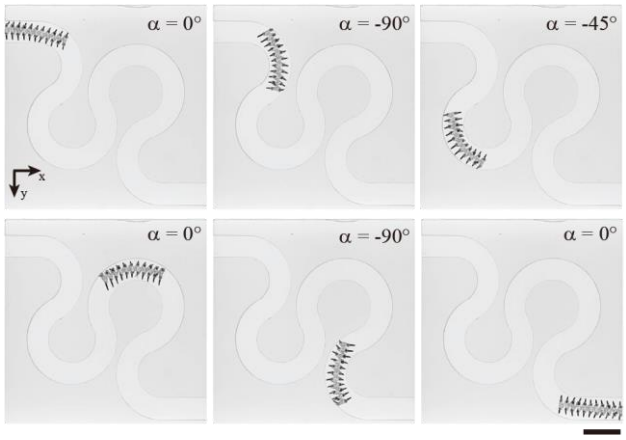

Figure 8. Locomotion of the robot in a tortuous environment. Scale bar: 10 mm.

V. Conclusion

In this work we present a millipede-inspired miniature soft robot capable of crawling with a traveling metachronal wave. Combing both simulation and experiment results, the underlying mechanism of metachronal wave generation and robot locomotion are elucidated. The specially designed body pattern endows the robot with flexibility in its body plane, enhancing its adaptability for efficient locomotion in tortuous environments.

With the improved adaptability, the miniature soft robot presented in this work shows great potential in biomedical applications within the tortuous cavities of the human body, including drug delivery, medical imaging, sensing, and sampling. To further advance its suitability for biomedical use, future research avenues may explore material interfaces tailored for tissue climbing, enabling the robot to access a broader range of regions. For applications within the gastrointestinal system, investigations into multimodal locomotion could offer solutions for adapting to both aquatic and terrestrial environments, enhancing the versatility of the robot. Additionally, the robot body may serve as a versatile platform for carrying drugs and contrast agents, which holds great potential for drug delivery and medical imaging applications.

Our future research endeavors will pivot towards the practical implementation of these miniature robots in biomedical contexts, emphasizing their utility and effectiveness in addressing real-world challenges and advancing the frontiers of biomedical robotics.

References

[1] M. Cianchetti, C. Laschi, A. Menciassi, and P. Dario, "Biomedical applications of soft robotics," Nat. Rev. Mater., vol. 3, no. 6, pp. 143–153, 2018.

[2] B. J. Nelson, I. K. Kaliakatsos, and J. J. Abbott, "Microrobots for minimally invasive medicine," Annu. Rev. Biomed. Eng., vol. 12, no. 1, pp. 55–85, 2010.

[3] M. Sitti et al., "Biomedical applications of untethered mobile Milli/microrobots," Proc. IEEE Inst. Electr. Electron. Eng., vol. 103, no. 2, pp. 205–224, 2015.

[4] T. Fukuda, "Cyborg and bionic systems: Signposting the future," Cyborg Bionic Syst., vol. 2020, p. 1310389, 2020.

[5] H. Chen, Y. Wang, Y. Liu, Q. Zou, and J. Yu, "Sensing of fluidic features using colloidal microswarms," ACS Nano, vol. 16, no. 10, pp. 16281–16291, 2022.

[6] J. Law et al., "Microrobotic swarms for selective embolization," Sci. Adv., vol. 8, no. 29, p. eabm5752, 2022.

[7] Z. Li, N. V. Myung, and Y. Yin, "Light-powered soft steam engines for self-adaptive oscillation and biomimetic swimming," Sci. Robot., vol. 6, no. 61, 2021.

[8] S. Wu, Y. Hong, Y. Zhao, J. Yin, and Y. Zhu, "Caterpillar-inspired soft crawling robot with distributed programmable thermal actuation," Sci. Adv., vol. 9, no. 12, 2023.

[9] Z. Yu et al., "Fast-response bioinspired near-infrared light-driven soft robot based on two-stage deformation," ACS Appl. Mater. Interfaces, vol. 14, no. 14, pp. 16649–16657, 2022.

[10] S. S. Nardekar and S.-J. Kim, "Untethered magnetic soft robot with ultra‐flexible wirelessly rechargeable micro‐supercapacitor as an onboard power source," Adv. Sci. (Weinh.), 2023.

[11] W. Hu, G. Z. Lum, M. Mastrangeli, and M. Sitti, "Small-scale soft-bodied robot with multimodal locomotion," Nature, vol. 554, no. 7690, pp. 81–85, 2018.

[12] M. Sitti, "Miniature soft robots — road to the clinic," Nat. Rev. Mater., vol. 3, no. 6, pp. 74–75, 2018.

[13] X. Du, J. Yu, "Image-Integrated Magnetic Actuation Systems for Localization and Remote Actuaion of Medical Miniature Robots: A Survey," IEEE Trans. Robot., vol. 39, no. 4, pp. 2549-2568, 2023.

[14] S. Palagi and P. Fischer, "Bioinspired microrobots," Nat. Rev. Mater., vol. 3, no. 6, pp. 113–124, 2018.

[15] L. Zhang, J. J. Abbott, L. Dong, B. E. Kratochvil, D. Bell, and B. J. Nelson, "Artificial bacterial flagella: Fabrication and magnetic control," Appl. Phys. Lett., vol. 94, no. 6, p. 064107, 2009.

[16] J. Yu, B. Wang, X. Du, Q. Wang, and L. Zhang, "Ultra-extensible ribbon-like magnetic microswarm," Nat. Commun., vol. 9, no. 1, p. 3260, 2018.

[17] J. Yu, D. Jin, K.-F. Chan, Q. Wang, K. Yuan, and L. Zhang, "Active generation and magnetic actuation of microrobotic swarms in bio-fluids," Nat. Commun., vol. 10, no. 1, p. 5631, 2019.

[18] H. Lu et al., "A bioinspired multilegged soft millirobot that functions in both dry and wet conditions," Nat. Commun., vol. 9, no. 1, p. 3944, 2018.

[19] V. K. Venkiteswaran, L. F. P. Samaniego, J. Sikorski, and S. Misra, "Bio-inspired terrestrial motion of magnetic soft millirobots," IEEE Robot. Autom. Lett., vol. 4, no. 2, pp. 1753–1759, 2019.

[20] Y. Wang, X. Du, H. Zhang, Q. Zou, J. Law, and J. Yu, "Amphibious miniature soft jumping robot with on-demand in-flight maneuver," Adv. Sci. (Weinh.), vol. 10, no. 18, p. e2207493, 2023.

[21] Z. Ren, W. Hu, X. Dong, and M. Sitti, "Multi-functional soft-bodied jellyfish-like swimming," Nat. Commun., vol. 10, no. 1, p. 2703, 2019.

[22] X. Dong et al., "Bioinspired cilia arrays with programmable nonreciprocal motion and metachronal coordination," Sci. Adv., vol. 6, no. 45, p. eabc9323, 2020.

[23] H. Gu et al., "Magnetic cilia carpets with programmable metachronal waves," Nat. Commun., vol. 11, no. 1, p. 2637, 2020.

[24] T. Wang, Z. Ren, W. Hu, M. Li, and M. Sitti, "Effect of body stiffness distribution on larval fish-like efficient undulatory swimming," Sci. Adv., vol. 7, no. 19, 2021.

[25] L. Yang et al., "Functionalized spiral-rolling millirobot for upstream swimming in blood vessel," Adv. Sci. (Weinh.), vol. 9, no. 16, p. e2200342, 2022.

[26] Y. Wang, H. Chen, J. Law, X. Du, and J. Yu, "Ultrafast miniature robotic swimmers with upstream motility," Cyborg Bionic Syst., vol. 4, p. 0015, 2023.

[27] Z. Ren et al., "Soft-bodied adaptive multimodal locomotion strategies in fluid-filled confined spaces," Sci. Adv., vol. 7, no. 27, 2021.

[28] Y. Wu, X. Dong, J.-K. Kim, C. Wang, and M. Sitti, "Wireless soft millirobots for climbing three-dimensional surfaces in confined spaces," Sci. Adv., vol. 8, no. 21, 2022.

[29] C. Wang, Y. Wu, X. Dong, M. Armacki, and M. Sitti, "In situ sensing physiological properties of biological tissues using wireless miniature soft robots," Sci. Adv., vol. 9, no. 23, 2023.

[30] Z. Chen et al., "A magnetic multi-layer soft robot for on-demand targeted adhesion," Nat. Commun., vol. 15, no. 1, pp. 1–13, 2024.

[31] X. Liu et al., "Magnetic soft microfiberbots for robotic embolization," Sci. Robot., vol. 9, no. 87, 2024.